Supplementary Note 1: The characterizations of single crystals of KV_3Sb_5 Single crystals of KV_3Sb_5 were grown via the self-flux method. K, V, and Sb were mixed by the ratio of 1:1:4.5 and sealed inside a Ta crucible. This Ta crucible was subsequently inside in evacuated quartz tube. The mixture was heated to 1000 ^{o}C, slowly cooled to 700 ^{o}C, and finally decanted by a centrifuge. Planar single crystals with typical dimensions of $2\times3\times0.3$ mm^3 were harvested at the bottom of the crucible.

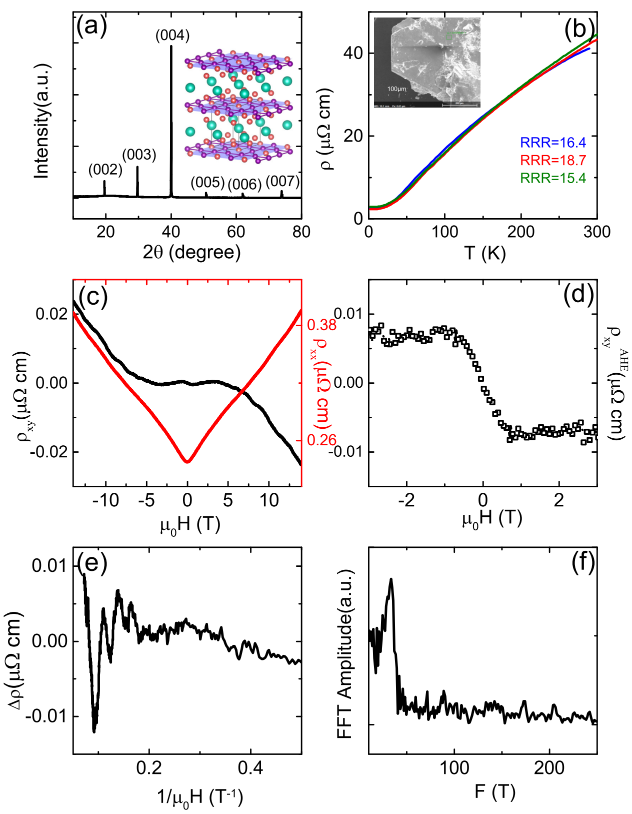

Crystal structure and elemental composition were confirmed by x-ray diffraction (XRD) and Energy Dispersive spectrometer(EDS). Sharp peaks in the XRD confirm high crystalline quality of the samples. The x-ray θ - 2θ diffraction spectrum for single crystal of KV_3Sb_5 is shown in Fig.

1 (a). The (00n) (n = 2, 4, 6, 8, and 10) diffraction peaks were observed indicating that the [001] direction is perpendicular to the plane of the crystals. As shown in the inset of Fig. 1 (a), KV_3Sb_5 exhibits layered structure with V ions forming kagome lattice.

Electrical transport measurements were performed in a Physical Properties Measurement System (PPMS Dynacool, Quantum design). Direct current (DC) magnetization and alternating current (AC) susceptibility measurements were performed in a Magnetic Property Measuring System (MPMS Quantum design).The temperature dependence of resistivity of KV_3Sb_5 are shown in Fig.1 (b) exhibiting metallic behavior with RRR varing from 15.4 to 18.7. The magnetoresistivity at 2 K with magnetic applied field along c axis ($H//c$) exhibits the quasi-linear field dependence shown in Fig .1 (c). The negative slope of Hall resistivity ρ_{ab} vs applied field H indicates the electron-type carriers agreeing with the results of angle resolved photoemission spectroscopy(ARPES). As shown in Fig. 1 (d), the anomalous Hall effect is observed around 1 T whose origin is still on puzzling. The obvious quantum oscillations are observed above 5 T and the Fast Fourier Transform spectrum reveals identifiable periods at 40 T.

Supplementary Note 2: The analysis of current jetting effect The Hall-bar devices were fabricated by exfoliating the single crystal of KV_3Sb_5 on to a SiO_2/Si substrate. Electronic contacts were added via patterned mask with photolithography subsequent growth of Ti/Au(10nm/100nm) layers.

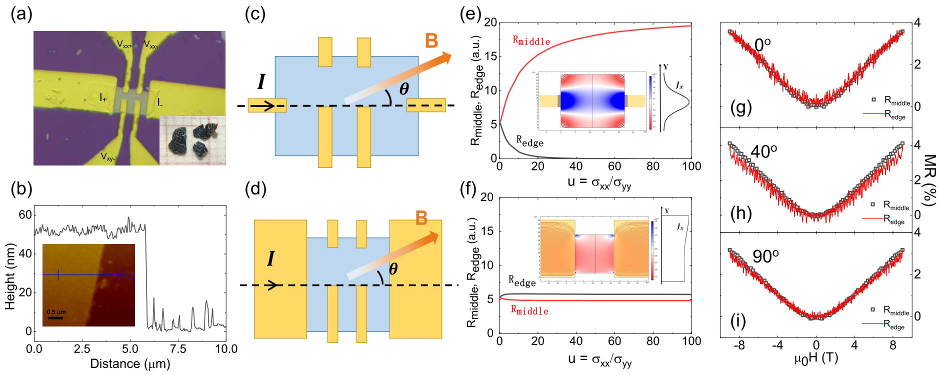

Current jetting refers to the focusing of the current density into a narrow beam ∥ H arising from the field induced anisotropy u of the conductivity (the drift of carriers transverse to B is suppressed relative to the longitudinal drift). This extrinsic contribution affecting the transport properties should be considered and analyzed during the our measurements. As the former research discussed, the contacts of irregular shape will lead to a much higher current density in the middle than that at the edge as shown in Figs. 2 (a) and (b) which is the main and usual origin of current jetting effect[1]. The distortion of current distribution can result in a negative magnetoresisitivity similar to that due to intrinsic contribution such as chiral anomaly but can be distinguished by measuring the resistivity in the middle and at edges. To avoid the geometry issue for transport measurements, we fabricate the single crystal into a regular rectangle device with symmetrical contacts as shown in the inset of Fig.2 (a). To check the homogeneity of the current flowing on our device, one couple of voltage contacts are located in the middle while another couple of voltage contacts are located at the edge shown in Fig.2 c and its inset. The simulation results are shown in Fig.2.(d). Compared to former research, this configuration lead to a negligible distortion of the current flowing with the anisotropy u=σ_{xy}/σ_{xx}. Considering the low in-plane anisotropy (about

1) in KV_3Sb_5, the distortion of the current flowing is much smaller in our measurements. We compared the field dependence of in-plane resistivity at various angles shown in Figs. 2 (e) - (f). The agreeable data acquired from measurements in the middle and at the edge indicates a small artificial contribution due to distortion of current flowing in our transport measurement.

Supplementary Note 3: The magnetoresistivity with rotating the applied field from a axis to c axis Fig. 3 shows the field dependence of magnetoresisitivity at various angles with rotating the applied field from a axis to c axis. The magnetoresistivity exhibits the almost linear dependence and the amplitude increases with the applied field rotating to c axis. It is noticed that no negative magnetoresisitivity is observed with I || H even the magnetoresisitivity is small. The failure of the observation negative magnetiresistivity relating to chiral anomaly is agreeable with other measurements results. We also checked the homogeneity of the current flowing by measuring the resistance in the middle and at the edge. The agreeable data indicate the small distortion of current flowing in our measurements.

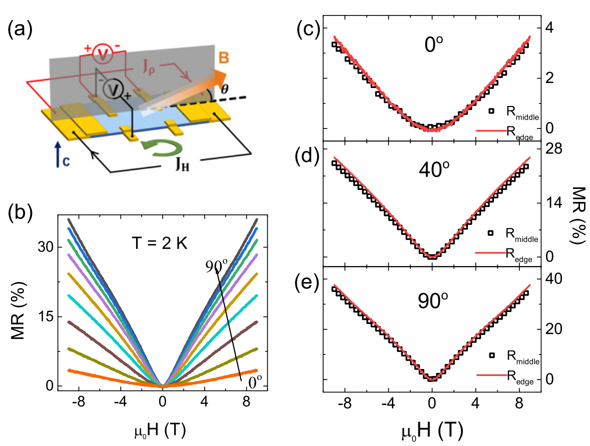

1. Liang, S. et al. Experimental Tests of the Chiral Anomaly Magnetoresistance in the Dirac-Weyl Semimetals Na_3Bi and GdPtBi. $Phys.Rev.X$ **8**, 031002 (2018).

Figure 1 (a): The x ray diffraction pattern of (00l) for single crystal of KV_3Sb_5. The inset: crystal structure of KV_3Sb_5. (b) temperature dependence of resistivity of KV_3Sb_5 (c) The field dependence of Hall (black line) and longitudinal (red line) resistivity with H$\|c$. (d) The anomalous Hall effect in zoomed (c). (e) The quantum oscillation acquired from ρ_{xy} by subtracting a background with H$\|c$. (f) Fast Fourier Transform spectrum of (e).

Figure 2 Simulation of current distribution and analysis of current jetting effect. (a) The optical image of the device for transport measurements. The inset: The single crystal of KV_3Sb_5 the for device fabrications. (b) Cross-sectional profile of the KV_3Sb_5 flake along the blue line in the inset of (b). The inset: Atomic force microscopy image of the area marked by the square in (a). (c) Schematic of measurements geometry with six contacts in ref[1]. d) The simulation results of the current distribution based on configuration in (c). The curves of resistivity measured in the middle (middle) and at edge (balck) vs the anisotropy of u = σ_{xx}/σ_{yy}. The inset: the contour of the current density distribution. The current density in the middle of the sample is much higher than that at edge. (e) Schematic of measurements geometry for in our sample. The current is along a axis direction and the applied field rotates within ab plane of the crystal. The inset: the picture of the device in our measurements. (f) The simulation results of the current distribution based on configuration in (e). The curves of resistivity measured in the middle and at edge vs the anisotropy of u = σ_{xx}/σ_{yy}. The inset: the contour of the current density distribution with large anisotropy of u = 2. The current density at edge is a little higher than that in the middle. (g), (h) and (i) The field dependence of resistivity measured in the middle (black) and at edge (red) with applied field rotating within ab plane of the crystal at 0°, 40°, and 90° respectively.

Figure 3 (a) schematic of measurements geometry with rotating the applied field from a axis to c axis. The resistivity measured in the middle and at edge of the sample are labeled as ch1 and ch2. (b) The field dependence of magnetoresitivity with at 0°, 20°, 30°, 40°, 50°, 60°, 70°, 80°, 90° rotating the applied field from a axis to c axis. (c), (d) and (e) The comparison of field dependent magnetoresistivity of ch1 and ch2 at 0°, 40°, 90° with measurements geometry in (a).